AIMS Mathematics

https://www.aimspress.com/journal/Math

AIMS Mathematics, 11(8): 24007–24032.
DOI: 10.3934/math.2026968
Received: 24 February 2026
Revised: 30 May 2026
Accepted: 09 June 2026
Published: 05 August 2026

Analytical solutions for the third extended fifth-order nonlinear equation and the nonlinear electrical transmission line model using the Sardar subequation method

Osama Alkhazaleh[1,*], Osama Ala'yed[2] and Abeer M. M. Jaradat[3]

[1] Department of Mathematics, Embry-Riddle Aeronautical University–Prescott Campus, Arizona 86301, USA

[2] Department of Mathematics, Jadara University, Jordan

[3] Department of Basic Sciences, Princess Sumaya University for Technology, Jordan

* **Correspondence:** Email: alkhazao@erau.edu.

Abstract: Nonlinear evolution equations (NLEEs) are widely used to model wave propagation and many other phenomena in physics and engineering. Obtaining exact analytical solutions of these equations remains important for understanding their mathematical structure and physical behavior. In this paper, the Sardar subequation method (SSM) is applied to derive new traveling-wave solutions for the third extended fifth-order nonlinear equation and the nonlinear electrical transmission-line model. By introducing a traveling-wave transformation, the governing partial differential equations are reduced to nonlinear ordinary differential equations, which are then solved using the proposed method. Several families of exact solutions are obtained in hyperbolic, trigonometric, and rational forms. To illustrate their physical characteristics, selected solutions are presented through three-dimensional (3D) surface and contour plots. The results show that the derived solutions exhibit different wave structures and provide additional analytical solutions for the models under consideration. Compared with many existing methods, the SSM offers a straightforward approach for constructing exact solutions without requiring restrictive assumptions. The findings presented in this work extend the known solution sets for these nonlinear models and provide useful analytical results for future studies on nonlinear wave propagation and related problems in mathematical physics.

Keywords: nonlinear wave equations; third extended fifth-order nonlinear equation; nonlinear electrical transmission line model; Sardar subequation method; analytical solutions
Mathematics Subject Classification: 35C07, 35Q51, 35Q53, 37K40

1. Introduction

Nonlinear evolution equations (NLEEs) play a fundamental role in modeling complex phenomena in various scientific disciplines, including fluid dynamics, optics, and electrical engineering. These equations often describe essential physical processes such as wave propagation, soliton interactions, and energy transport in nonlinear media. Due to their mathematical richness and physical relevance, obtaining exact analytical solutions of NLEEs remains a central pursuit in applied mathematics and mathematical physics. Over the past decades, numerous analytical and semi-analytical techniques have been proposed to investigate the solution structures of NLEEs, including the hyperbolic tangent-cotangent method [1–3], the sine-Gordon expansion method [4–6], the $\frac{G'}{G}$-expansion method [7–9], the Darboux transformation [10–12], the Hirota bilinear method [13–15], the generalized Kudryashov technique [16, 17], the modified F-expansion method, the modified generalized Riccati equation technique, the modified generalized exponential rational function technique [18], the $\frac{1}{G'}$, the modified $\frac{G'}{G^2}$, and the extended direct algebraic methods [19], and the Bernoulli sub-equation neural network method [20].

Among these methods, the Sardar subequation method (SSM) has recently emerged as an efficient and accessible approach for constructing exact traveling-wave solutions of nonlinear differential equations [21]. The SSM is based on the formulation of simpler auxiliary subequations, which significantly reduces the analytical complexity of the solution procedure. Its notable strengths include flexibility, simplicity, and computational efficiency, particularly in comparison with methods such as the generalized Kudryashov technique and the Hirota bilinear approach, which often involve more elaborate balancing procedures or complex symbolic computations. Moreover, the SSM is applicable to a broad class of partial differential equations, including problems where some conventional methods may not be readily applicable. In particular, it does not require strict integrability conditions or the prior existence of soliton structures, significantly broadening its applicability. The method is further distinguished by its ability to generate a diverse range of exact solutions, including soliton, solitary wave, periodic, and rational forms. In addition, it yields bright, dark, and singular soliton solutions that effectively capture the characteristic behaviors of nonlinear dispersive systems [22–24]. Despite these advantages, the SSM, like other subequation-based approaches, depends on appropriate balance conditions and parameter constraints. Consequently, it may not capture all possible solution structures, particularly for equations involving non-polynomial nonlinearities or cases where the homogeneous balance yields non-integer values. Nevertheless, its simplicity, flexibility, and computational efficiency make it a valuable tool for exploring nonlinear dynamical systems.

In this work, we employ the SSM to investigate two significant nonlinear models. The first model is the third extended fifth-order nonlinear equation given by

$$v_{zzz} - v_{zyyyy} - v_{zxx} - 4(v_y\, v_{yz})_y = 0, \tag{1.1}$$

where $v = v(x, y, z)$ represents the wave field. This equation arises in nonlinear wave theory and plays an important role in describing the interaction between nonlinearity and higher-order dispersion effects, particularly in fluid mechanics and shallow-water dynamics [25, 26].

The second model considered in this study is the nonlinear electrical transmission line equation, expressed as

$$v_{zz} - \sigma(v^2)_{zz} + \beta(v^3)_{zz} - u_0^2\delta_2^2\, v_{xx} - k_0^2\delta_1^2\, v_{yy} - \frac{u_0^2\delta_2^4}{12}\, v_{xxxx} - \frac{k_0^2\delta_1^4}{12}\, v_{yyyy} = 0, \tag{1.2}$$

where $v = v(x, y, z)$ denotes the voltage in an electrical transmission line. This model also describes wave propagation in network structures and nonlinear signal transmission systems. The parameters σ and β represent the strengths of quadratic and cubic nonlinearities, respectively. The constants $u_0^2 = \frac{1}{L_1 C_0}$ and $k_0^2 = \frac{1}{L_2 C_0}$ determine the propagation speeds in the longitudinal and transverse directions, where L_1 and L_2 are inductances and C_0 is the linear capacitance per unit length. The parameters δ_1 and δ_2 denote the spatial discretization in the longitudinal and transverse directions, introducing anisotropy and higher-order dispersion effects associated with the lattice structure of the transmission line. This equation is fundamental in modeling nonlinear voltage propagation in electrical and electromagnetic systems [27, 28].

Although a variety of analytical methods have been applied to these models, such as Hirota's direct method [29], the Riccati equation rational expansion method [30], the sine-Gordon expansion method [13], the exponential function method [21], the first and second simple methods [31], and the Jacobi elliptic function expansion method [32], the SSM has not yet been systematically applied to these models, and its potential to uncover additional exact solutions remains largely untapped. Motivated by this, the present study applies the SSM to derive exact soliton solutions for both models, which are of significant interest across various scientific domains. The main contribution of this study lies in the systematic application of the SSM to the aforementioned models to derive previously unreported families of exact traveling-wave solutions. These solutions include a variety of functional forms, such as hyperbolic, trigonometric, and rational expressions, as well as different types of soliton structures. The obtained results not only enrich the theoretical understanding of the underlying nonlinear systems but also provide insights into their physical behavior in relevant applications. Furthermore, symbolic computations are supported by graphical visualizations generated using Maple, including three-dimensional (3D) and contour plots, which illustrate the dynamical features of the obtained solutions.

The primary objectives of this study are summarized as follows:

(1) To construct new exact traveling-wave solutions of the considered nonlinear models using the SSM.
(2) To analyze the structural and physical characteristics of the obtained solutions.
(3) To demonstrate the effectiveness and versatility of the SSM in solving complex nonlinear evolution equations.

The remainder of this paper is organized as follows. Section 2 provides an overview of the SSM and outlines its fundamental principles. Section 3 applies the method to the considered nonlinear models and derives exact solutions. Section 4 discusses the analysis of the derived solutions and their physical interpretations. Finally, Section 5 concludes the article by summarizing the main findings and describing potential future research directions.

2. Preliminaries and method description

2.1. Overview of the SSM

The SSM is a systematic analytical technique for deriving exact traveling-wave solutions of nonlinear differential equations. By reducing the original nonlinear partial differential equation (NPDE) to a solvable nonlinear ordinary differential equation (NODE), the method enables the construction of soliton, periodic, and rational function solutions. Due to its flexibility and efficiency, the SSM has been successfully applied in mathematical physics, fluid dynamics, optical communications, and electrical engineering, where nonlinear wave behavior is of central importance.

To describe the method, consider a general NPDE of the form

$$P(v, v_x, v_y, v_z, v_{xx}, v_{yy}, v_{zz}, \dots) = 0, \tag{2.1}$$

where $v(x, y, z)$ is the dependent variable and P is a nonlinear operator. The first step is to apply the traveling-wave transformation

$$v(x, y, z) = V(s), \qquad s = r(x + y - cz), \tag{2.2}$$

where c represents the wave speed, r is a scaling parameter, and s represents a moving coordinate frame. This transformation reduces the multidimensional problem to a single-variable equation, thereby simplifying the analysis. Using the chain rule, the derivatives of v with respect to the original variables are expressed in terms of s as follows:

$$v_x = rV', \quad v_y = rV', \quad v_z = -rc\,V', \quad v_{xx} = r^2V'', \quad v_{yy} = r^2V'', \quad v_{zz} = r^2c^2V'', \dots, \tag{2.3}$$

where the prime denotes differentiation with respect to s. Substituting (2.2) and (2.3) into the original NPDE reduces it to a NODE of the form

$$P^*(V, V', V'', \dots) = 0. \tag{2.4}$$

The SSM assumes that the solution $V(s)$ can be expressed as a finite polynomial expansion in terms of an auxiliary function $\psi(s)$, namely

$$V(s) = \sum_{i=0}^{n} \omega_i \psi^i(s), \tag{2.5}$$

where ω_i are constants to be determined. The function $\psi(s)$ satisfies the nonlinear subequation

$$(\psi')^2 = a + b\psi^2 + \psi^4, \tag{2.6}$$

where a and b are real constants. The positive integer n in (2.5) is determined using the homogeneous balance principle between the highest-order derivative terms and the nonlinear terms in (2.4). If the degree of $V(s)$ is defined as $D[V(s)] = n$, then the degree of a general term is given by

$$D\left[V^q\left(\frac{d^jV}{ds^j}\right)^m\right] = nq + m(j + n),$$

which follows from the definition of the degree of $V(s)$ and its derivatives. Balancing the dominant terms in the reduced equation determines the appropriate value of n. Substituting the trial solution (2.5) along with (2.6) into (2.4) yields a system of algebraic equations in terms of the unknown parameters ω_i, a, b, r, and c. Solving this system provides explicit forms of the traveling-wave solutions. This procedure offers a systematic framework for deriving a wide range of exact solutions and facilitates the analysis of diverse nonlinear wave behaviors.

The admissible forms of $\psi(s)$ arising from different parameter choices in (2.6) are summarized below.

Case 1: If $a = 0$ and $b > 0$, then

$$\begin{aligned}\psi_1^{\pm}(s) &= \pm\sqrt{-pqb}\,\mathrm{sech}_{pq}(\sqrt{b}\,s),\\ \psi_2^{\pm}(s) &= \pm\sqrt{pqb}\,\mathrm{csch}_{pq}(\sqrt{b}\,s),\end{aligned}$$

where

$$\mathrm{sech}_{pq}(s) = \frac{2}{pe^{s} + qe^{-s}}, \qquad \mathrm{csch}_{pq}(s) = \frac{2}{pe^{s} - qe^{-s}}.$$

Case 2: If $a = 0$ and $b < 0$, then

$$\begin{aligned}\psi_3^{\pm}(s) &= \pm\sqrt{-pqb}\,\sec_{pq}(\sqrt{-b}\,s),\\ \psi_4^{\pm}(s) &= \pm\sqrt{-pqb}\,\csc_{pq}(\sqrt{-b}\,s),\end{aligned}$$

where

$$\sec_{pq}(s) = \frac{2}{pe^{is} + qe^{-is}}, \quad \csc_{pq}(s) = \frac{2i}{pe^{is} - qe^{-is}}.$$

Case 3: If $b < 0$ and $a = \frac{b^2}{4}$, then

$$\begin{aligned}\psi_5^{\pm}(s) &= \pm\sqrt{\tfrac{-b}{2}}\,\tanh_{pq}\left(\sqrt{\tfrac{-b}{2}}\,s\right),\\ \psi_6^{\pm}(s) &= \pm\sqrt{\tfrac{-b}{2}}\,\coth_{pq}\left(\sqrt{\tfrac{-b}{2}}\,s\right),\\ \psi_7^{\pm}(s) &= \pm\sqrt{\frac{-b}{2}}\left(\tanh_{pq}\left(\sqrt{-2b}\,s\right) \pm i\sqrt{pq}\,\mathrm{sech}_{pq}\left(\sqrt{-2b}\,s\right)\right),\\ \psi_8^{\pm}(s) &= \pm\sqrt{\frac{-b}{2}}\left(\coth_{pq}\left(\sqrt{-2b}\,s\right) \pm \sqrt{pq}\,\mathrm{csch}_{pq}\left(\sqrt{-2b}\,s\right)\right),\\ \psi_9^{\pm}(s) &= \pm\sqrt{\frac{-b}{8}}\left(\tanh_{pq}\left(\sqrt{\tfrac{-b}{8}}\,s\right) + \coth_{pq}\left(\sqrt{\tfrac{-b}{8}}\,s\right)\right),\end{aligned}$$

where

$$\tanh_{pq}(s) = \frac{pe^{s} - qe^{-s}}{pe^{s} + qe^{-s}}, \quad \coth_{pq}(s) = \frac{pe^{s} + qe^{-s}}{pe^{s} - qe^{-s}}.$$

Case 4: If $b > 0$ and $a = \frac{b^2}{4}$, then

$$\begin{aligned}
\psi_{10}^{\pm}(s) &= \pm\sqrt{\tfrac{b}{2}}\tan_{pq}\left(\sqrt{\tfrac{b}{2}}\,s\right),\\
\psi_{11}^{\pm}(s) &= \pm\sqrt{\tfrac{b}{2}}\cot_{pq}\left(\sqrt{\tfrac{b}{2}}\,s\right),\\
\psi_{12}^{\pm}(s) &= \pm\sqrt{\tfrac{b}{2}}\left(\tan_{pq}\left(\sqrt{2b}\,s\right) \pm \sqrt{pq}\sec_{pq}\left(\sqrt{2b}\,s\right)\right),\\
\psi_{13}^{\pm}(s) &= \pm\sqrt{\tfrac{b}{2}}\left(\cot_{pq}\left(\sqrt{2b}\,s\right) \pm \sqrt{pq}\csc_{pq}\left(\sqrt{2b}\,s\right)\right),\\
\psi_{14}^{\pm}(s) &= \pm\sqrt{\tfrac{b}{8}}\left(\tan_{pq}\left(\sqrt{\tfrac{b}{8}}\,s\right) - \cot_{pq}\left(\sqrt{\tfrac{b}{8}}\,s\right)\right),
\end{aligned}$$

where

$$\tan_{pq}(s) = -i\frac{pe^{is} - qe^{-is}}{pe^{is} + qe^{-is}}, \quad \cot_{pq}(s) = i\frac{pe^{is} + qe^{-is}}{pe^{is} - qe^{-is}}.$$

These solution forms will be employed in the subsequent sections to construct exact traveling-wave solutions for the considered models, demonstrating the versatility and effectiveness of the SSM in analyzing nonlinear physical systems.

2.2. *Model assumptions*

To ensure clarity in the formulation and interpretation of the mathematical models considered in this study, we summarize the main assumptions underlying the analysis:

- **Continuum approximation:** The physical systems are modeled as continuous media, where the dependent variable $v(x, y, z)$ represents a smooth field (e.g., wave elevation or voltage) varying continuously in space and time.
- **Traveling-wave structure:** The solutions are assumed to admit a traveling-wave form $v(x, y, z) = V(s)$, where $s = r(x + y - cz)$. This reduces the governing partial differential equations to ordinary differential equations.
- **Nonlinearity and dispersion balance:** The models incorporate both nonlinear and dispersive effects, and it is assumed that these effects interact to produce stable wave structures such as solitons or periodic waves.
- **Parameter constancy:** All physical parameters (e.g., b, r, σ, β, k_0, δ_1, δ_2) are assumed to be constant, representing homogeneous media.
- **Negligible dissipation:** The models do not include dissipative effects such as resistance or damping, implying that energy is conserved within the system.
- **Small perturbation framework:** In the stability analysis, perturbations are assumed to be sufficiently small ($0 < \epsilon \ll 1$), allowing linearization of the governing equations.
- **Well-posed boundary behavior:** For localized solutions, it is assumed that $v(x, y, z) \to 0$ as $|s| \to \infty$, ensuring finite energy and physical admissibility.

3. Applications

In this section, the SSM is employed to derive new exact solutions for the third extended fifth-order nonlinear model and the (2+1)-dimensional nonlinear electrical transmission line model.

3.1. The third extended fifth-order nonlinear model

In this subsection, we apply the SSM to derive new exact traveling-wave solutions of the third extended fifth-order nonlinear model given in (1.1). By applying the traveling-wave transformation (2.2) and its corresponding derivatives (2.3), Eq (1.1) is reduced to the following NODE:

$$(-c^3 + c)V^{(3)} + r^2 cV^{(5)} + 4cr(V'V'')' = 0. \tag{3.1}$$

Integrating once with respect to s gives

$$(-c^3 + c)V'' + r^2 cV^{(4)} + 4crV'V'' = C_1, \tag{3.2}$$

where C_1 is an integration constant. A second integration yields

$$(-c^3 + c)V' + r^2 cV^{(3)} + 2cr(V')^2 = C_1 s + C_2, \tag{3.3}$$

where C_2 is another constant of integration. Assuming localized soliton solutions, the integration constants can be set to zero for simplicity [33]. Accordingly, Eq (3.3) reduces to

$$r^2 V^{(3)} + 2r(V')^2 + (1 - c^2)V' = 0. \tag{3.4}$$

To simplify the analysis, we introduce the substitution

$$F = V',$$

which transforms Eq (3.4) into

$$r^2 F'' + 2rF^2 + (1 - c^2)F = 0. \tag{3.5}$$

Applying the homogeneous balance principle and balancing F'' and F^2 yields $2 + n = 2n$, from which $n = 2$ is obtained. Consequently, substituting $n = 2$ into the trial form (2.5) gives the following expression for the solution function:

$$F = \omega_0 + \omega_1\psi + \omega_2\psi^2. \tag{3.6}$$

Substituting (3.6) into (3.5) leads to the algebraic system

$$\begin{aligned}
&2ar^2\omega_2 + 2r\omega_0^2 + (1 - c^2)\omega_0 = 0,\\
&br^2\omega_1 + 4r\omega_0\omega_1 + (1 - c^2)\omega_1 = 0,\\
&4br^2\omega_2 + 4r\omega_0\omega_2 + 2r\omega_1^2 + (1 - c^2)\omega_2 = 0,\\
&2r^2\omega_1 + 4r\omega_1\omega_2 = 0,\\
&6r^2\omega_2 + 2r\omega_2^2 = 0.
\end{aligned} \tag{3.7}$$

Solving this system symbolically using Mathematica yields several sets of parameter values, which can be classified as follows:

For Cases 1 and 2:

$$\begin{aligned}
&\omega_0 = -2\,b\,r, \omega_1 = 0,\ \omega_2 = -3\,r, c = \pm\sqrt{1 - 4\,b\,r^2},\\
&\omega_0 = 0, \omega_1 = 0,\ \omega_2 = -3\,r, c = \pm\sqrt{1 + 4\,b\,r^2}.
\end{aligned} \tag{3.8}$$

For Cases 3 and 4:

$$\begin{aligned} &\omega_0 = -\frac{3\,b\,r}{2}, \omega_1 = 0,\ \omega_2 = -3\,r, c = \pm\sqrt{1-2\,b\,r^2},\\ &\omega_0 = -\frac{b\,r}{2}, \omega_1 = 0,\ \omega_2 = -3\,r, c = \pm\sqrt{1+2\,b\,r^2}. \end{aligned} \tag{3.9}$$

Substituting these parameter sets, together with the corresponding solutions of the auxiliary Eq (2.6), into (3.6), and then integrating with respect to s, yields explicit exact traveling-wave solutions of the original nonlinear model. To illustrate the physical characteristics of the obtained solutions, representative 3D surface and contour plots corresponding to selected solutions are presented in Figures 1–4.

Case 1: If $a = 0$ and $b > 0$, then

$$v_1^{\pm}(x,y,z) = -2\,b\,r^2\left(x+y\pm\sqrt{1-4\,b\,r^2}\,z\right) + 3\,r\sqrt{b}\,\tanh_{pq}\left(\sqrt{b}\,r\left(x+y\pm\sqrt{1-4\,b\,r^2}\,z\right)\right), \tag{3.10}$$

$$v_2^{\pm}(x,y,z) = -2\,b\,r^2\left(x+y\pm\sqrt{1-4\,b\,r^2}\,z\right) + 3\,r\sqrt{b}\,\coth_{pq}\left(\sqrt{b}\,r\left(x+y\pm\sqrt{1-4\,b\,r^2}\,z\right)\right), \tag{3.11}$$

$$v_3^{\pm}(x,y,z) = 3\,r\sqrt{b}\,\tanh_{pq}\left(\sqrt{b}\,r\left(x+y\pm\sqrt{1+4\,b\,r^2}\,z\right)\right), \tag{3.12}$$

$$v_4^{\pm}(x,y,z) = 3\,r\sqrt{b}\,\coth_{pq}\left(\sqrt{b}\,r\left(x+y\pm\sqrt{1+4\,b\,r^2}\,z\right)\right). \tag{3.13}$$

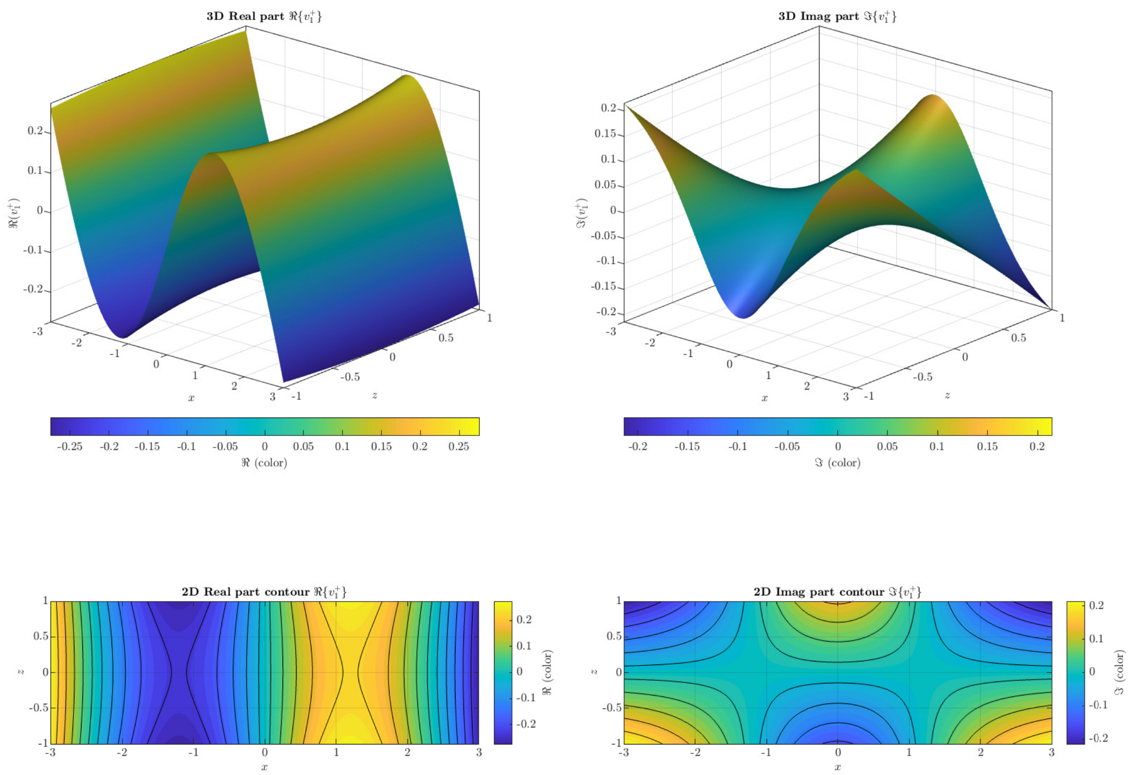

Figure 1. 3D surface and contour plots of the real and imaginary parts of v_1^+ in (3.10).

Case 2: If $a = 0$ and $b < 0$, then

$$v_5^{\pm}(x,y,z) = -2\,b\,r^2\left(x+y\pm\sqrt{1-4\,b\,r^2}\,z\right) - 3\,r\sqrt{-b}\,\tan_{pq}\left(\sqrt{-b}\,r\left(x+y\pm\sqrt{1-4\,b\,r^2}\,z\right)\right), \quad (3.14)$$

$$v_6^{\pm}(x,y,z) = -2\,b\,r^2\left(x+y\pm\sqrt{1-4\,b\,r^2}\,z\right) + 3\,r\sqrt{-b}\,\cot_{pq}\left(\sqrt{-b}\,r\left(x+y\pm\sqrt{1-4\,b\,r^2}\,z\right)\right). \quad (3.15)$$

$$v_7^{\pm}(x,y,z) = -3\,r\sqrt{-b}\,\tan_{pq}\left(\sqrt{-b}\,r\left(x+y\pm\sqrt{1+4\,b\,r^2}\,z\right)\right), \quad (3.16)$$

$$v_8^{\pm}(x,y,z) = 3\,r\sqrt{-b}\,\cot_{pq}\left(\sqrt{-b}\,r\left(x+y\pm\sqrt{1+4\,b\,r^2}\,z\right)\right). \quad (3.17)$$

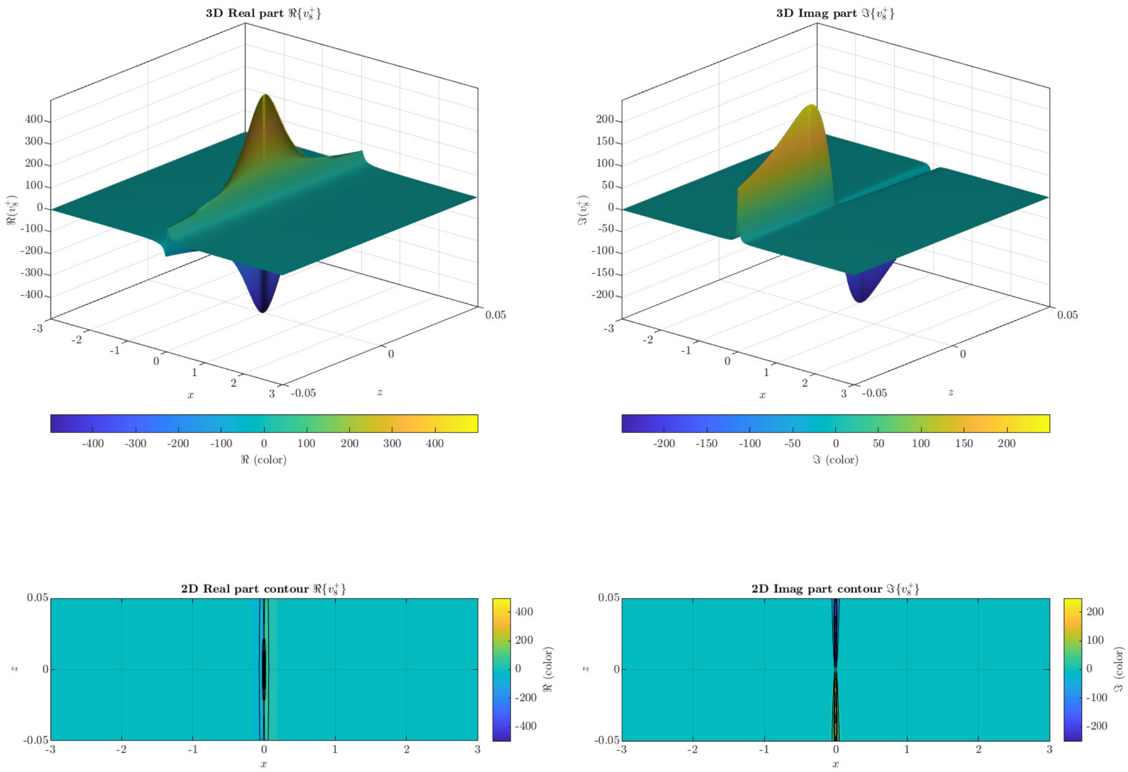

Figure 2. 3D and contour plots of the real and imaginary parts of v_8^+ in (3.17).

Case 3: If $a = \dfrac{b^2}{4}$ and $b < 0$, then

$$v_9^{\pm}(x,y,z) = 3\,r\sqrt{\frac{-b}{2}}\,\tanh_{pq}\left(\sqrt{\frac{-b}{2}}\,r\left(x+y\pm\sqrt{1-2\,b\,r^2}\,z\right)\right), \quad (3.18)$$

$$v_{10}^{\pm}(x,y,z) = 3\,r\sqrt{\frac{-b}{2}}\,\coth_{pq}\left(\sqrt{\frac{-b}{2}}\,r\left(x+y\pm\sqrt{1-2\,b\,r^2}\,z\right)\right), \quad (3.19)$$

$$v_{11}^{\pm}(x,y,z) = 3\,r\sqrt{\frac{-b}{2}}\Big[\tanh_{pq}\Big(\sqrt{-2\,b}\,r\big(x+y\pm\sqrt{1-2\,b\,r^2}\,z\big)\Big) \pm i\,\sqrt{p\,q}\,\text{sech}_{pq}\Big(\sqrt{-2b}\,r\big(x+y\pm\sqrt{1-2\,b\,r^2}\,z\big)\Big)\Big], \tag{3.20}$$

$$v_{12}^{\pm}(x,y,z) = -3\,r\sqrt{\frac{-b}{2}}\Big[\coth_{pq}\Big(\sqrt{-2\,b}\,r\big(x+y\pm\sqrt{1-2\,b\,r^2}\,z\big)\Big) \pm\sqrt{p\,q}\,\text{csch}_{pq}\Big(\sqrt{-2b}\,r\big(x+y\pm\sqrt{1-2\,b\,r^2}\,z\big)\Big)\Big], \tag{3.21}$$

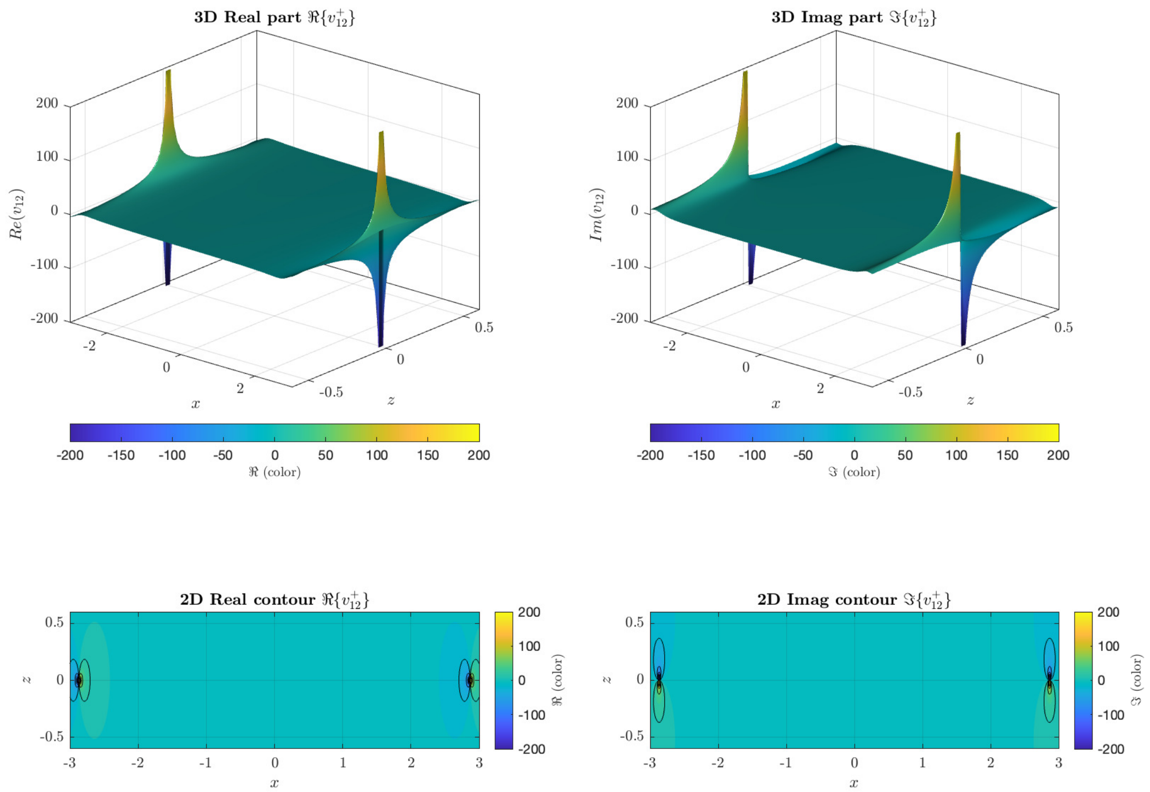

Figure 3. 3D and contour plots of the real and imaginary parts of v_{12}^{+} in (3.21).

$$v_{13}^{\pm}(x,y,z) = 3r\sqrt{\frac{-b}{8}}\Bigg[\tanh_{pq}\Bigg(\sqrt{\frac{-b}{8}}\,r\big(x+y\pm\sqrt{1-2br^2}\,z\big)\Bigg) + \coth_{pq}\Bigg(\sqrt{\frac{-b}{8}}\,r\big(x+y\pm\sqrt{1-2br^2}\,z\big)\Bigg)\Bigg], \tag{3.22}$$

$$v_{14}^{\pm}(x,y,z) = br^2\big(x+y\pm\sqrt{1+2br^2}\,z\big) + 3r\sqrt{\frac{-b}{2}}\,\tanh_{pq}\Bigg(\sqrt{\frac{-b}{2}}\,r\big(x+y\pm\sqrt{1+2br^2}\,z\big)\Bigg), \tag{3.23}$$

$$v_{15}^{\pm}(x,y,z) = br^2\left(x+y\pm\sqrt{1+2br^2}\,z\right)+3r\sqrt{\frac{-b}{2}}\,\coth_{pq}\left(\sqrt{\frac{-b}{2}}\,r\left(x+y\pm\sqrt{1+2br^2}\,z\right)\right). \tag{3.24}$$

$$\begin{aligned} v_{16}^{\pm}(x,y,z) = {} & b\,r^2\left(x+y\pm\sqrt{1+2\,b\,r^2}\,z\right)+3\,r\sqrt{\frac{-b}{2}}\Big[\tanh_{pq}\left(\sqrt{-2\,b}\,r\left(x+y\pm\sqrt{1+2\,b\,r^2}\,z\right)\right) \\ & \pm i\sqrt{p\,q}\,\mathrm{sech}_{pq}\left(\sqrt{-2b}\,r\left(x+y\pm\sqrt{1+2\,b\,r^2}\,z\right)\right)\Big], \end{aligned} \tag{3.25}$$

$$\begin{aligned} v_{17}^{\pm}(x,y,z) = {} & b\,r^2\left(x+y\pm\sqrt{1+2\,b\,r^2}\,z\right)-3\,r\sqrt{\frac{-b}{2}}\Big[\coth_{pq}\left(\sqrt{-2\,b}\,r\left(x+y\pm\sqrt{1+2\,b\,r^2}\,z\right)\right) \\ & \pm\sqrt{p\,q}\,\mathrm{csch}_{pq}\left(\sqrt{-2b}\,r\left(x+y\pm\sqrt{1+2\,b\,r^2}\,z\right)\right)\Big], \end{aligned} \tag{3.26}$$

$$\begin{aligned} v_{18}^{\pm}(x,y,z) = {} & b\,r^2\left(x+y\pm\sqrt{1+2\,b\,r^2}\,z\right)+3\,r\sqrt{\frac{-b}{8}}\Big[\tanh_{pq}\left(\sqrt{\frac{-b}{8}}\,r\left(x+y\pm\sqrt{1+2\,b\,r^2}\,z\right)\right) \\ & +\coth_{pq}\left(\sqrt{\frac{-b}{8}}\,r\left(x+y\pm\sqrt{1+2\,b\,r^2}\,z\right)\right)\Big]. \end{aligned} \tag{3.27}$$

Case 4: If $a=\dfrac{b^2}{4}$ and $b>0$, then

$$v_{19}^{\pm}(x,y,z) = 3\,r\sqrt{\frac{b}{2}}\,\tan_{pq}\left(\sqrt{\frac{b}{2}}\,r\left(x+y\pm\sqrt{1-2\,b\,r^2}\,z\right)\right), \tag{3.28}$$

$$v_{20}^{\pm}(x,y,z) = 3\,r\sqrt{\frac{b}{2}}\,\cot_{pq}\left(\sqrt{\frac{b}{2}}\,r\left(x+y\pm\sqrt{1-2\,b\,r^2}\,z\right)\right), \tag{3.29}$$

$$\begin{aligned} v_{21}^{\pm}(x,y,z) = {} & -3\,r\sqrt{\frac{b}{2}}\Big[\tan_{pq}\left(\sqrt{2\,b}\,r\left(x+y\pm\sqrt{1-2\,b\,r^2}\,z\right)\right) \\ & \pm\sqrt{p\,q}\,\sec_{pq}\left(\sqrt{2\,b}\,r\left(x+y\pm\sqrt{1-2\,b\,r^2}\,z\right)\right)\Big], \end{aligned} \tag{3.30}$$

$$\begin{aligned} v_{22}^{\pm}(x,y,z) = {} & -3\,r\sqrt{\frac{b}{2}}\Big[-\cot_{pq}\left(\sqrt{2\,b}\,r\left(x+y\pm\sqrt{1-2\,b\,r^2}\,z\right)\right) \\ & \pm\sqrt{p\,q}\,\csc_{pq}\left(\sqrt{2b}\,r\left(x+y\pm\sqrt{1-2\,b\,r^2}\,z\right)\right)\Big], \end{aligned} \tag{3.31}$$

$$\begin{aligned} v_{23}^{\pm}(x,y,z) = {} & 3\,r\sqrt{\frac{b}{8}}\Big[\tan_{pq}\left(\sqrt{\frac{b}{8}}\,r\left(x+y\pm\sqrt{1-2\,b\,r^2}\,z\right)\right) \\ & -\cot_{pq}\left(\sqrt{\frac{b}{8}}\,r\left(x+y\pm\sqrt{1-2\,b\,r^2}\,z\right)\right)\Big], \end{aligned} \tag{3.32}$$

$$v_{24}^{\pm}(x,y,z) = b\,r^2\left(x+y\pm\sqrt{1+2\,b\,r^2}\,z\right)-3\,r\sqrt{\frac{b}{2}}\,\tan_{pq}\left(\sqrt{\frac{b}{2}}\,r\left(x+y\pm\sqrt{1+2\,b\,r^2}\,z\right)\right), \tag{3.33}$$

$$v_{25}^{\pm}(x,y,z) = b\,r^2\left(x+y\pm\sqrt{1+2\,b\,r^2}\,z\right)-3\,r\sqrt{\frac{b}{2}}\,\cot_{pq}\left(\sqrt{\frac{b}{2}}\,r\left(x+y\pm\sqrt{1+2\,b\,r^2}\,z\right)\right), \tag{3.34}$$

$$v_{26}^{\pm}(x,y,z) = b\,r^2\left(x+y\pm\sqrt{1+2\,b\,r^2}\,z\right) - 3\,r\sqrt{\frac{b}{2}}\Big[\tan_{pq}\Big(\sqrt{2}\,b\,r\left(x+y\pm\sqrt{1+2\,b\,r^2}\,z\right)\Big) \pm\sqrt{p\,q}\,\sec_{pq}\Big(\sqrt{2}\,b\,r\left(x+y\pm\sqrt{1+2\,b\,r^2}\,z\right)\Big)\Big], \tag{3.35}$$

$$v_{27}^{\pm}(x,y,z) = b\,r^2\left(x+y\pm\sqrt{1+2\,b\,r^2}\,z\right) + 3\,r\sqrt{\frac{b}{2}}\Big[\cot_{pq}\Big(\sqrt{2}\,b\,r\left(x+y\pm\sqrt{1+2\,b\,r^2}\,z\right)\Big) \pm\sqrt{p\,q}\,\csc_{pq}\Big(\sqrt{2b}\,r\left(x+y\pm\sqrt{1+2\,b\,r^2}\,z\right)\Big)\Big], \tag{3.36}$$

$$v_{28}^{\pm}(x,y,z) = b\,r^2\left(x+y\pm\sqrt{1+2\,b\,r^2}\,z\right) - 3\,r\sqrt{\frac{b}{8}}\left[\tan_{pq}\left(\sqrt{\frac{b}{8}}\,r\left(x+y\pm\sqrt{1+2\,b\,r^2}\,z\right)\right) - \cot_{pq}\left(\sqrt{\frac{b}{8}}\,r\left(x+y\pm\sqrt{1+2\,b\,r^2}\,z\right)\right)\right]. \tag{3.37}$$

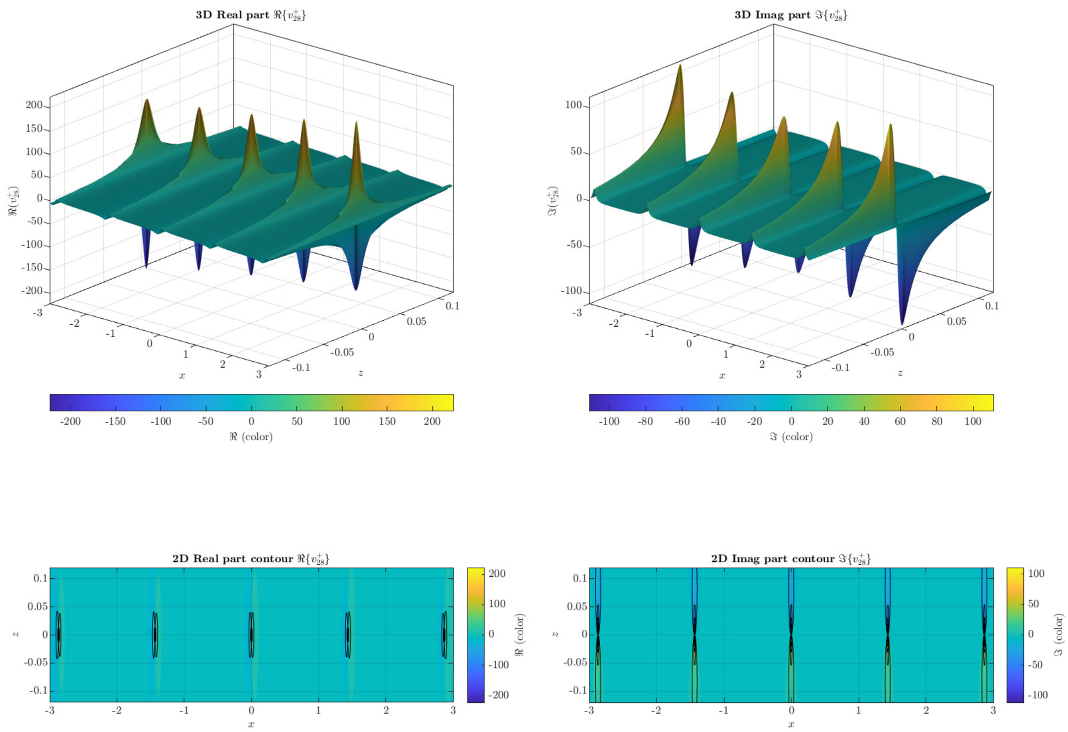

Figure 4. 3D and contour plots of the real and imaginary parts of v_{28}^{+} in (3.37).

These exact solutions provide insights into the structural properties of the underlying model and may serve as benchmark solutions for evaluating the accuracy and reliability of future numerical and approximate analytical methods. In addition, they further confirm the effectiveness of the SSM in constructing exact solutions for higher-order nonlinear evolution equations.

3.2. The (2+1)-dimensional nonlinear electrical transmission line model

In this subsection, we derive new solutions for the (2+1)-dimensional nonlinear electrical transmission line model given in (1.2). By applying the transformation (2.2), Eq (1.2) is reduced to the following NODE:

$$r^2\left(c^2-k_0^2\delta_1^2-u_0^2\delta_2^2\right)V''-2r^2c^2\sigma\left(VV'\right)'+3r^2c^2\beta\left(V^2V'\right)'-\frac{1}{12}r^4\left(k_0^2\delta_1^4+u_0^2\delta_2^4\right)V^{(4)}=0. \tag{3.38}$$

Integrating once with respect to s gives

$$r^2\left(c^2-k_0^2\delta_1^2-u_0^2\delta_2^2\right)V'-2r^2c^2\sigma VV'+3r^2c^2\beta V^2V'-\frac{1}{12}r^4\left(k_0^2\delta_1^4+u_0^2\delta_2^4\right)V^{(3)}=C_1, \tag{3.39}$$

where C_1 is an integration constant. A second integration yields

$$r^2\left(c^2-k_0^2\delta_1^2-u_0^2\delta_2^2\right)V-r^2c^2\sigma V^2+r^2c^2\beta V^3-\frac{1}{12}r^4\left(k_0^2\delta_1^4+u_0^2\delta_2^4\right)V''=C_1s+C_2, \tag{3.40}$$

where C_2 is another constant of integration. Assuming localized soliton solutions, the integration constants can be set to zero for simplicity [33]. Accordingly, Eq (3.40) reduces to

$$\left(c^2-k_0^2\delta_1^2-u_0^2\delta_2^2\right)V-c^2\sigma V^2+c^2\beta V^3-\frac{1}{12}r^2\left(k_0^2\delta_1^4+u_0^2\delta_2^4\right)V''=0. \tag{3.41}$$

Applying the homogeneous balance principle and balancing V'' and V^3 yields $3n=2+n$, from which $n=1$ is obtained. Consequently, substituting $n=1$ into the trial form (2.5) gives the following expression for the solution function

$$V=\omega_0+\omega_1\psi. \tag{3.42}$$

Substituting (3.42) into (3.41) leads to the algebraic system

$$\begin{aligned}
&\left(c^2-k_0^2\delta_1^2-u_0^2\delta_2^2\right)\omega_0-c^2\sigma\omega_0^2+c^2\beta\omega_0^3=0,\\
&\left(c^2-k_0^2\delta_1^2-u_0^2\delta_2^2\right)\omega_1-\frac{1}{12}br^2\left(k_0^2\delta_1^4+u_0^2\delta_2^4\right)\omega_1-2c^2\sigma\omega_0\omega_1+3c^2\beta\omega_0^2\omega_1=0,\\
&-c^2\sigma\omega_1^2+3c^2\beta\omega_0\omega_1^2=0,\quad -\frac{1}{6}r^2\left(k_0^2\delta_1^4+u_0^2\delta_2^4\right)\omega_1+c^2\beta\omega_1^3=0.
\end{aligned} \tag{3.43}$$

Solving this system symbolically using Mathematica yields several sets of parameter values, which can be classified as follows.

$$\begin{aligned}
&\omega_0=\frac{\sigma}{3\beta}, && \omega_1=\pm\frac{ir\sqrt{2\sigma^2-9\beta}\sqrt{k_0^2\delta_1^4+u_0^2\delta_2^4}}{\sqrt{54\beta^2\left(k_0^2\delta_1^2+u_0^2\delta_2^2\right)}},\\
&b=\frac{12\sigma^2\left(k_0^2\delta_1^2+u_0^2\delta_2^2\right)}{r^2(2\sigma^2-9\beta)\left(k_0^2\delta_1^4+u_0^2\delta_2^4\right)}, && c=\pm\frac{3\sqrt{-\beta\left(k_0^2\delta_1^2+u_0^2\delta_2^2\right)}}{\sqrt{2\sigma^2-9\beta}}.
\end{aligned} \tag{3.44}$$

Substituting these parameter sets, together with the corresponding solutions of the auxiliary equation (2.6) into (3.42) yields explicit exact traveling-wave solutions of the original nonlinear model. To further illustrate the physical characteristics of the obtained solutions for the nonlinear electrical transmission line model, representative 3D surface and contour plots corresponding to selected solutions are presented in Figures 5–8.

Case 1: If $a = 0$ and $b > 0$, then

$$\begin{aligned} v_1^{\pm}(x,y,z) =& \frac{\sigma}{3\beta} \pm \frac{ir\sqrt{2\sigma^2-9\beta}\sqrt{k_0^2\delta_1^4+u_0^2\delta_2^4}}{\sqrt{54\beta^2k_0^2\delta_1^2+54\beta^2u_0^2\delta_2^2}} \times \sqrt{-pq\frac{12\sigma^2(k_0^2\delta_1^2+u_0^2\delta_2^2)}{r^2(2\sigma^2-9\beta)(k_0^2\delta_1^4+u_0^2\delta_2^4)}} \\ & \times \operatorname{sech}_{pq}\left(\sqrt{\frac{12\sigma^2(k_0^2\delta_1^2+u_0^2\delta_2^2)}{r^2(2\sigma^2-9\beta)(k_0^2\delta_1^4+u_0^2\delta_2^4)}}\,r\left(x+y\pm\frac{3\sqrt{-\beta(k_0^2\delta_1^2+u_0^2\delta_2^2)}}{\sqrt{2\sigma^2-9\beta}}z\right)\right), \end{aligned} \tag{3.45}$$

$$\begin{aligned} v_2^{\pm}(x,y,z) =& \frac{\sigma}{3\beta} \pm \frac{ir\sqrt{2\sigma^2-9\beta}\sqrt{k_0^2\delta_1^4+u_0^2\delta_2^4}}{\sqrt{54\beta^2k_0^2\delta_1^2+54\beta^2u_0^2\delta_2^2}} \times \sqrt{pq\frac{12\sigma^2(k_0^2\delta_1^2+u_0^2\delta_2^2)}{r^2(2\sigma^2-9\beta)(k_0^2\delta_1^4+u_0^2\delta_2^4)}} \\ & \times \operatorname{csch}_{pq}\left(\sqrt{\frac{12\sigma^2(k_0^2\delta_1^2+u_0^2\delta_2^2)}{r^2(2\sigma^2-9\beta)(k_0^2\delta_1^4+u_0^2\delta_2^4)}}\,r\left(x+y\pm\frac{3\sqrt{-\beta(k_0^2\delta_1^2+u_0^2\delta_2^2)}}{\sqrt{2\sigma^2-9\beta}}z\right)\right). \end{aligned} \tag{3.46}$$

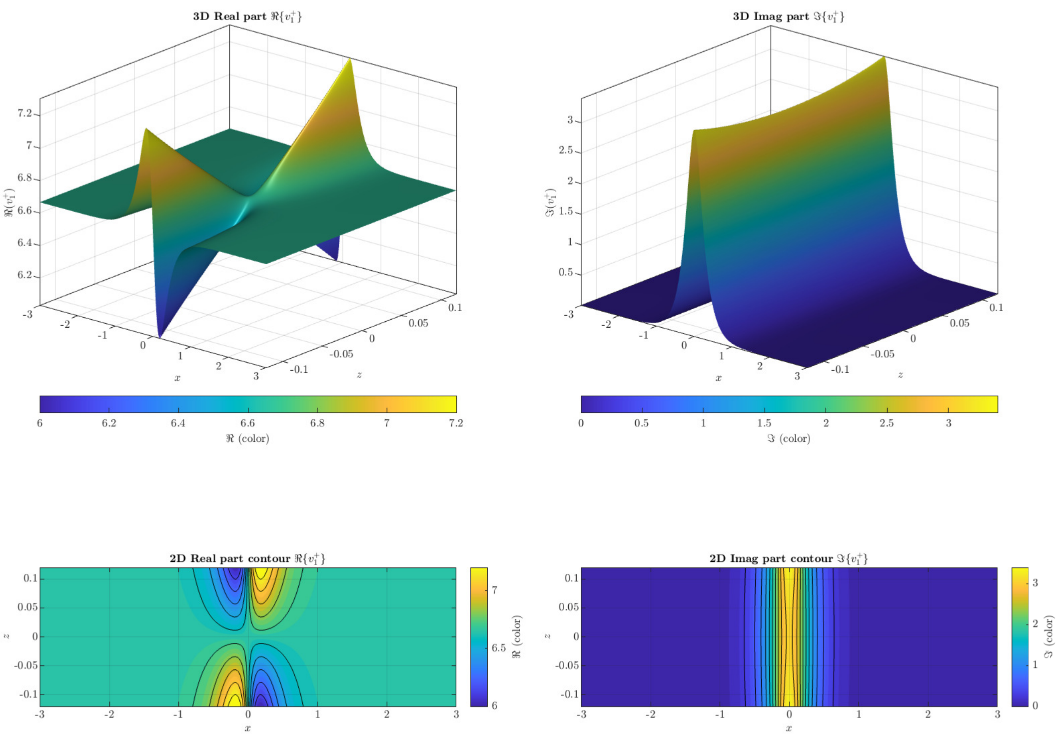

Figure 5. 3D and contour plots of the real and imaginary parts of v_1^+ in (3.45).

Case 2: If $a = 0$ and $b < 0$, then

$$
\begin{aligned}
v_3^{\pm}(x,y,z) =& \frac{\sigma}{3\beta} \pm \frac{i\,r\,\sqrt{2\sigma^2-9\beta}\,\sqrt{k_0^2\delta_1^4+u_0^2\delta_2^4}}{\sqrt{54\beta^2k_0^2\delta_1^2+54\beta^2u_0^2\delta_2^2}} \times \sqrt{\frac{-pq\,12\sigma^2(k_0^2\delta_1^2+u_0^2\delta_2^2)}{r^2(2\sigma^2-9\beta)(k_0^2\delta_1^4+u_0^2\delta_2^4)}} \\
& \times \sec_{pq}\left(\sqrt{\frac{-12\sigma^2(k_0^2\delta_1^2+u_0^2\delta_2^2)}{r^2(2\sigma^2-9\beta)(k_0^2\delta_1^4+u_0^2\delta_2^4)}}\; r\left(x+y \pm \frac{3\sqrt{-\beta(k_0^2\delta_1^2+u_0^2\delta_2^2)}}{\sqrt{2\sigma^2-9\beta}}z\right)\right),
\end{aligned}
\tag{3.47}
$$

$$
\begin{aligned}
v_4^{\pm}(x,y,z) =& \frac{\sigma}{3\beta} \pm \frac{ir\,\sqrt{2\sigma^2-9\beta}\,\sqrt{k_0^2\delta_1^4+u_0^2\delta_2^4}}{\sqrt{54\beta^2k_0^2\delta_1^2+54\beta^2u_0^2\delta_2^2}} \times \sqrt{-\,p\,q\,\frac{12\sigma^2(k_0^2\delta_1^2+u_0^2\delta_2^2)}{r^2(2\sigma^2-9\beta)(k_0^2\delta_1^4+u_0^2\delta_2^4)}} \\
& \times \csc_{pq}\left(\sqrt{-\frac{12\sigma^2(k_0^2\delta_1^2+u_0^2\delta_2^2)}{r^2(2\sigma^2-9\beta)(k_0^2\delta_1^4+u_0^2\delta_2^4)}}\; r\left(x+y \pm \frac{3\sqrt{-\,\beta(k_0^2\delta_1^2+u_0^2\delta_2^2)}}{\sqrt{2\sigma^2-9\beta}}\,z\right)\right).
\end{aligned}
\tag{3.48}
$$

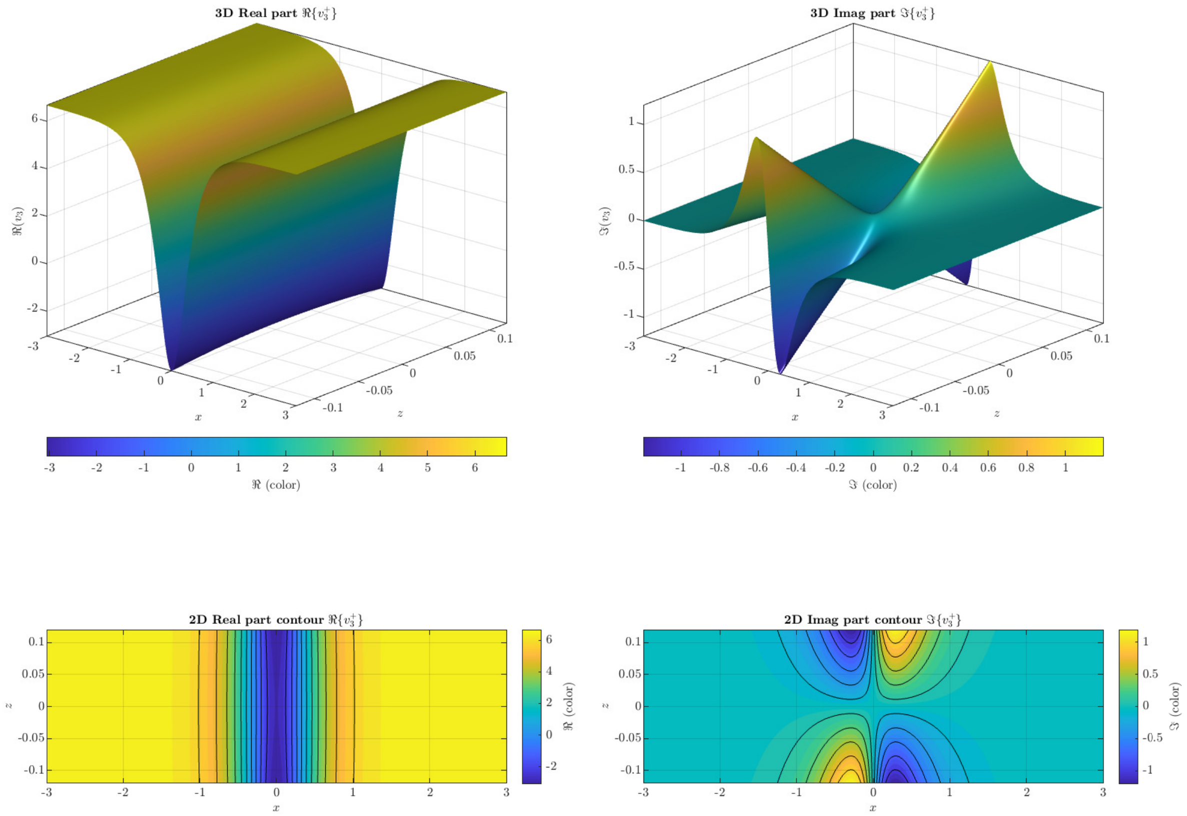

Figure 6. 3D and contour plots of the real and imaginary parts of v_3^+ in (3.47).

Case 3: If $b < 0$ and $a = \frac{b^2}{4}$, then

$$\begin{aligned} v_5^{\pm}(x,y,z) =& \frac{\sigma}{3\beta} \pm \frac{ir\sqrt{2\sigma^2-9\beta}\sqrt{k_0^2\delta_1^4+u_0^2\delta_2^4}}{\sqrt{54\beta^2k_0^2\delta_1^2+54\beta^2u_0^2\delta_2^2}} \times \sqrt{-\frac{6\sigma^2(k_0^2\delta_1^2+u_0^2\delta_2^2)}{r^2(2\sigma^2-9\beta)(k_0^2\delta_1^4+u_0^2\delta_2^4)}} \\ & \times \tanh_{pq}\left(\sqrt{-\frac{6\sigma^2(k_0^2\delta_1^2+u_0^2\delta_2^2)}{r^2(2\sigma^2-9\beta)(k_0^2\delta_1^4+u_0^2\delta_2^4)}}r\left(x+y\pm\frac{3\sqrt{-\beta(k_0^2\delta_1^2+u_0^2\delta_2^2)}}{\sqrt{2\sigma^2-9\beta}}z\right)\right), \end{aligned} \tag{3.49}$$

$$\begin{aligned} v_6^{\pm}(x,y,z) =& \frac{\sigma}{3\beta} \pm \frac{ir\sqrt{2\sigma^2-9\beta}\sqrt{k_0^2\delta_1^4+u_0^2\delta_2^4}}{\sqrt{54\beta^2k_0^2\delta_1^2+54\beta^2u_0^2\delta_2^2}} \times \sqrt{-\frac{6\sigma^2(k_0^2\delta_1^2+u_0^2\delta_2^2)}{r^2(2\sigma^2-9\beta)(k_0^2\delta_1^4+u_0^2\delta_2^4)}} \\ & \times \coth_{pq}\left(\sqrt{-\frac{6\sigma^2(k_0^2\delta_1^2+u_0^2\delta_2^2)}{r^2(2\sigma^2-9\beta)(k_0^2\delta_1^4+u_0^2\delta_2^4)}}r\left(x+y\pm\frac{3\sqrt{-\beta(k_0^2\delta_1^2+u_0^2\delta_2^2)}}{\sqrt{2\sigma^2-9\beta}}z\right)\right), \end{aligned} \tag{3.50}$$

$$\begin{aligned} v_7^{\pm}(x,y,z) =& \frac{\sigma}{3\beta} \pm \frac{ir\sqrt{2\sigma^2-9\beta}\sqrt{k_0^2\delta_1^4+u_0^2\delta_2^4}}{\sqrt{54\beta^2k_0^2\delta_1^2+54\beta^2u_0^2\delta_2^2}} \Bigg[\pm\sqrt{\frac{-6\sigma^2(k_0^2\delta_1^2+u_0^2\delta_2^2)}{r^2(2\sigma^2-9\beta)(k_0^2\delta_1^4+u_0^2\delta_2^4)}} \\ & \times \tanh_{pq}\left(\sqrt{\frac{-24\sigma^2(k_0^2\delta_1^2+u_0^2\delta_2^2)}{r^2(2\sigma^2-9\beta)(k_0^2\delta_1^4+u_0^2\delta_2^4)}}r\left(x+y\pm\frac{3\sqrt{-\beta(k_0^2\delta_1^2+u_0^2\delta_2^2)}}{\sqrt{2\sigma^2-9\beta}}z\right)\right) \\ & \pm i\sqrt{pq}\,\mathrm{sech}_{pq}\left(\sqrt{\frac{-24\sigma^2(k_0^2\delta_1^2+u_0^2\delta_2^2)}{r^2(2\sigma^2-9\beta)(k_0^2\delta_1^4+u_0^2\delta_2^4)}}r\left(x+y\pm\frac{3\sqrt{-\beta(k_0^2\delta_1^2+u_0^2\delta_2^2)}}{\sqrt{2\sigma^2-9\beta}}z\right)\right)\Bigg], \end{aligned} \tag{3.51}$$

$$\begin{aligned} v_8^{\pm}(x,y,z) =& \frac{\sigma}{3\beta} \pm \frac{ir\sqrt{2\sigma^2-9\beta}\sqrt{k_0^2\delta_1^4+u_0^2\delta_2^4}}{\sqrt{54\beta^2k_0^2\delta_1^2+54\beta^2u_0^2\delta_2^2}} \Bigg[\pm\sqrt{\frac{-6\sigma^2(k_0^2\delta_1^2+u_0^2\delta_2^2)}{r^2(2\sigma^2-9\beta)(k_0^2\delta_1^4+u_0^2\delta_2^4)}} \\ & \times \coth_{pq}\left(\sqrt{\frac{-24\sigma^2(k_0^2\delta_1^2+u_0^2\delta_2^2)}{r^2(2\sigma^2-9\beta)(k_0^2\delta_1^4+u_0^2\delta_2^4)}}r\left(x+y\pm\frac{3\sqrt{-\beta(k_0^2\delta_1^2+u_0^2\delta_2^2)}}{\sqrt{2\sigma^2-9\beta}}z\right)\right) \\ & \pm \sqrt{pq}\,\mathrm{csch}_{pq}\left(\sqrt{\frac{-24\sigma^2(k_0^2\delta_1^2+u_0^2\delta_2^2)}{r^2(2\sigma^2-9\beta)(k_0^2\delta_1^4+u_0^2\delta_2^4)}}r\left(x+y\pm\frac{3\sqrt{-\beta(k_0^2\delta_1^2+u_0^2\delta_2^2)}}{\sqrt{2\sigma^2-9\beta}}z\right)\right)\Bigg], \end{aligned} \tag{3.52}$$

$$
\begin{aligned}
v_9^{\pm}(x,y,z) =& \frac{\sigma}{3\beta} \pm \frac{ir\sqrt{2\sigma^2-9\beta}\sqrt{k_0^2\delta_1^4+u_0^2\delta_2^4}}{\sqrt{54\beta^2k_0^2\delta_1^2+54\beta^2u_0^2\delta_2^2}}\Bigg[\pm\sqrt{\frac{-12\sigma^2(k_0^2\delta_1^2+u_0^2\delta_2^2)}{8r^2(2\sigma^2-9\beta)(k_0^2\delta_1^4+u_0^2\delta_2^4)}} \\
&\times \tanh_{pq}\left(\sqrt{\frac{-12\sigma^2(k_0^2\delta_1^2+u_0^2\delta_2^2)}{8r^2(2\sigma^2-9\beta)(k_0^2\delta_1^4+u_0^2\delta_2^4)}}r\left(x+y\pm\frac{3\sqrt{-\beta(k_0^2\delta_1^2+u_0^2\delta_2^2)}}{\sqrt{2\sigma^2-9\beta}}z\right)\right) \\
&+ \coth_{pq}\left(\sqrt{\frac{-12\sigma^2(k_0^2\delta_1^2+u_0^2\delta_2^2)}{8r^2(2\sigma^2-9\beta)(k_0^2\delta_1^4+u_0^2\delta_2^4)}}r\left(x+y\pm\frac{3\sqrt{-\beta(k_0^2\delta_1^2+u_0^2\delta_2^2)}}{\sqrt{2\sigma^2-9\beta}}z\right)\right)\Bigg].
\end{aligned}
\tag{3.53}
$$

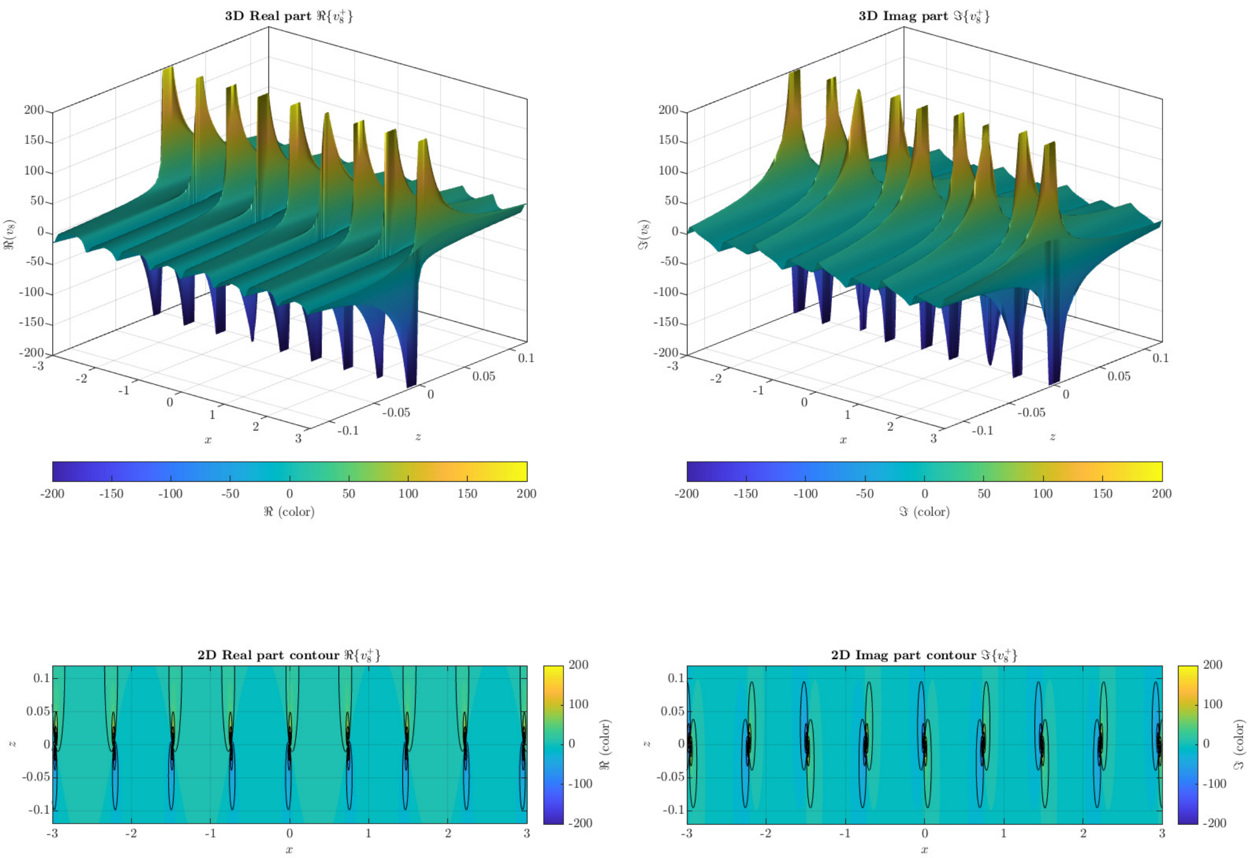

Figure 7. 3D and contour plots of the real and imaginary parts of v_8^+ in (3.52).

Case 4: If $b > 0$ and $a = \frac{b^2}{4}$, then

$$\begin{aligned} v_{10}^{\pm}(x,y,z) =& \frac{\sigma}{3\beta} \pm \frac{ir\sqrt{2\sigma^2-9\beta}\sqrt{k_0^2\delta_1^4+u_0^2\delta_2^4}}{\sqrt{54\beta^2k_0^2\delta_1^2+54\beta^2u_0^2\delta_2^2}} \times \sqrt{\frac{6\sigma^2(k_0^2\delta_1^2+u_0^2\delta_2^2)}{r^2(2\sigma^2-9\beta)(k_0^2\delta_1^4+u_0^2\delta_2^4)}} \\ & \times \tan_{pq}\left(\sqrt{\frac{6\sigma^2(k_0^2\delta_1^2+u_0^2\delta_2^2)}{r^2(2\sigma^2-9\beta)(k_0^2\delta_1^4+u_0^2\delta_2^4)}}r\left(x+y\pm\frac{3\sqrt{-\beta(k_0^2\delta_1^2+u_0^2\delta_2^2)}}{\sqrt{2\sigma^2-9\beta}}z\right)\right), \end{aligned} \tag{3.54}$$

$$\begin{aligned} v_{11}^{\pm}(x,y,z) =& \frac{\sigma}{3\beta} \pm \frac{ir\sqrt{2\sigma^2-9\beta}\sqrt{k_0^2\delta_1^4+u_0^2\delta_2^4}}{\sqrt{54\beta^2k_0^2\delta_1^2+54\beta^2u_0^2\delta_2^2}} \times \sqrt{\frac{6\sigma^2(k_0^2\delta_1^2+u_0^2\delta_2^2)}{r^2(2\sigma^2-9\beta)(k_0^2\delta_1^4+u_0^2\delta_2^4)}} \\ & \times \cot_{pq}\left(\sqrt{\frac{6\sigma^2(k_0^2\delta_1^2+u_0^2\delta_2^2)}{r^2(2\sigma^2-9\beta)(k_0^2\delta_1^4+u_0^2\delta_2^4)}}r\left(x+y\pm\frac{3\sqrt{-\beta(k_0^2\delta_1^2+u_0^2\delta_2^2)}}{\sqrt{2\sigma^2-9\beta}}z\right)\right), \end{aligned} \tag{3.55}$$

$$\begin{aligned} v_{12}^{\pm}(x,y,z) =& \frac{\sigma}{3\beta} \pm \frac{ir\sqrt{2\sigma^2-9\beta}\sqrt{k_0^2\delta_1^4+u_0^2\delta_2^4}}{\sqrt{54\beta^2k_0^2\delta_1^2+54\beta^2u_0^2\delta_2^2}}\left[\pm\sqrt{\frac{6\sigma^2(k_0^2\delta_1^2+u_0^2\delta_2^2)}{r^2(2\sigma^2-9\beta)(k_0^2\delta_1^4+u_0^2\delta_2^4)}}\right. \\ & \times \tan_{pq}\left(\sqrt{\frac{24\sigma^2(k_0^2\delta_1^2+u_0^2\delta_2^2)}{r^2(2\sigma^2-9\beta)(k_0^2\delta_1^4+u_0^2\delta_2^4)}}r\left(x+y\pm\frac{3\sqrt{-\beta(k_0^2\delta_1^2+u_0^2\delta_2^2)}}{\sqrt{2\sigma^2-9\beta}}z\right)\right) \\ & \left.\pm\sqrt{pq}\sec_{pq}\left(\sqrt{\frac{24\sigma^2(k_0^2\delta_1^2+u_0^2\delta_2^2)}{r^2(2\sigma^2-9\beta)(k_0^2\delta_1^4+u_0^2\delta_2^4)}}r\left(x+y\pm\frac{3\sqrt{-\beta(k_0^2\delta_1^2+u_0^2\delta_2^2)}}{\sqrt{2\sigma^2-9\beta}}z\right)\right)\right], \end{aligned} \tag{3.56}$$

$$\begin{aligned} v_{13}^{\pm}(x,y,z) =& \frac{\sigma}{3\beta} \pm \frac{ir\sqrt{2\sigma^2-9\beta}\sqrt{k_0^2\delta_1^4+u_0^2\delta_2^4}}{\sqrt{54\beta^2k_0^2\delta_1^2+54\beta^2u_0^2\delta_2^2}}\left[\pm\sqrt{\frac{6\sigma^2(k_0^2\delta_1^2+u_0^2\delta_2^2)}{r^2(2\sigma^2-9\beta)(k_0^2\delta_1^4+u_0^2\delta_2^4)}}\right. \\ & \times \cot_{pq}\left(\sqrt{\frac{24\sigma^2(k_0^2\delta_1^2+u_0^2\delta_2^2)}{r^2(2\sigma^2-9\beta)(k_0^2\delta_1^4+u_0^2\delta_2^4)}}r\left(x+y\pm\frac{3\sqrt{-\beta(k_0^2\delta_1^2+u_0^2\delta_2^2)}}{\sqrt{2\sigma^2-9\beta}}z\right)\right) \\ & \left.\pm\sqrt{pq}\csc_{pq}\left(\sqrt{\frac{24\sigma^2(k_0^2\delta_1^2+u_0^2\delta_2^2)}{r^2(2\sigma^2-9\beta)(k_0^2\delta_1^4+u_0^2\delta_2^4)}}r\left(x+y\pm\frac{3\sqrt{-\beta(k_0^2\delta_1^2+u_0^2\delta_2^2)}}{\sqrt{2\sigma^2-9\beta}}z\right)\right)\right], \end{aligned} \tag{3.57}$$

$$v_{14}^{\pm}(x,y,z) = \frac{\sigma}{3\beta} \pm \frac{ir\sqrt{2\sigma^2-9\beta}\sqrt{k_0^2\delta_1^4+u_0^2\delta_2^4}}{\sqrt{54\beta^2k_0^2\delta_1^2+54\beta^2u_0^2\delta_2^2}}\Bigg[\pm\sqrt{\frac{12\sigma^2(k_0^2\delta_1^2+u_0^2\delta_2^2)}{8r^2(2\sigma^2-9\beta)(k_0^2\delta_1^4+u_0^2\delta_2^4)}}$$
$$\times \tan_{pq}\left(\sqrt{\frac{12\sigma^2(k_0^2\delta_1^2+u_0^2\delta_2^2)}{8r^2(2\sigma^2-9\beta)(k_0^2\delta_1^4+u_0^2\delta_2^4)}}r\left(x+y\pm\frac{3\sqrt{-\beta(k_0^2\delta_1^2+u_0^2\delta_2^2)}}{\sqrt{2\sigma^2-9\beta}}z\right)\right)$$
$$-\cot_{pq}\left(\sqrt{\frac{12\sigma^2(k_0^2\delta_1^2+u_0^2\delta_2^2)}{8r^2(2\sigma^2-9\beta)(k_0^2\delta_1^4+u_0^2\delta_2^4)}}r\left(x+y\pm\frac{3\sqrt{-\beta(k_0^2\delta_1^2+u_0^2\delta_2^2)}}{\sqrt{2\sigma^2-9\beta}}z\right)\right)\Bigg]. \tag{3.58}$$

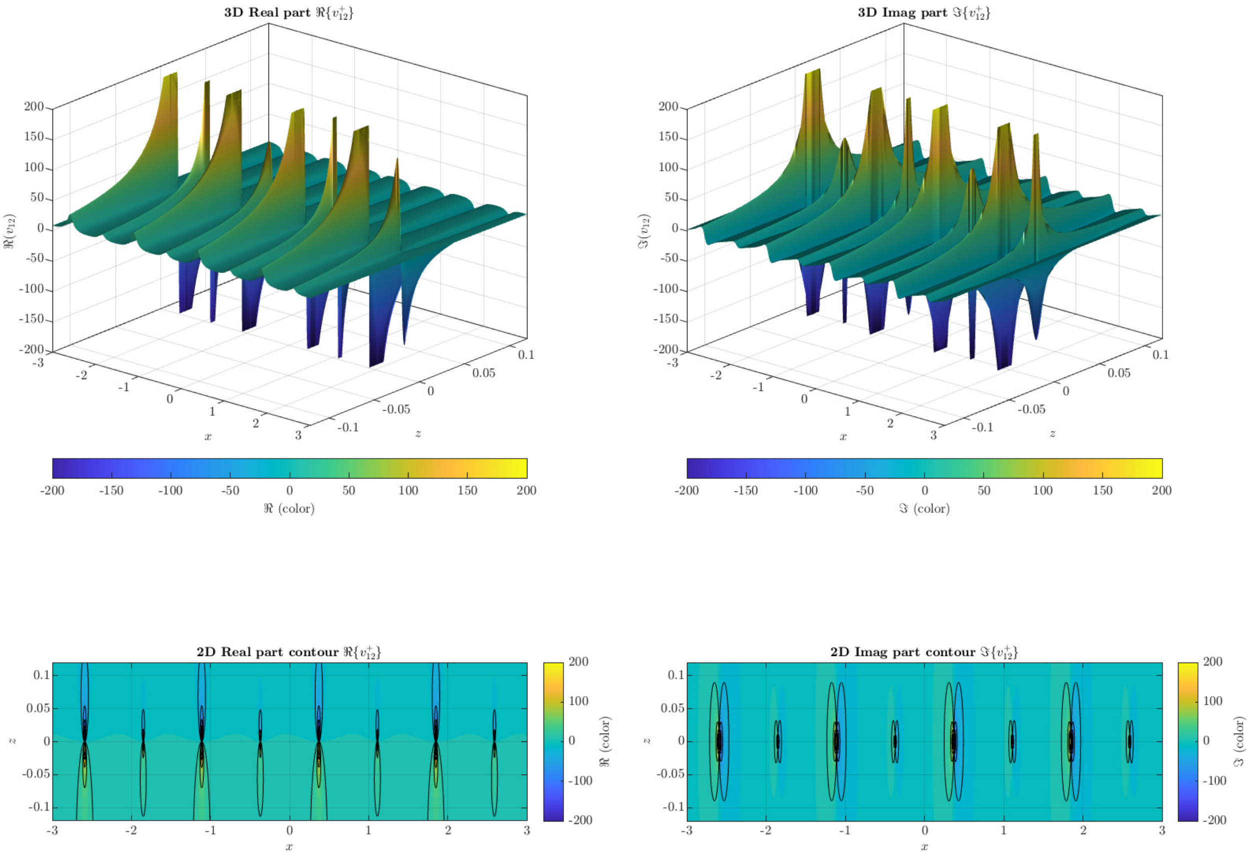

Figure 8. 3D and contour plots of the real and imaginary parts of v_{12}^+ in (3.56).

These exact solutions provide insights into the structural properties of the underlying model and may serve as benchmark solutions for evaluating the accuracy and reliability of future numerical and approximate analytical methods. In addition, they further confirm the effectiveness of the SSM in constructing exact solutions for higher-order nonlinear evolution equations.

4. Results and discussion

The analytical expressions obtained through the SSM reveal a rich variety of traveling-wave behaviors for both nonlinear models considered. To illustrate these behaviors, representative solutions are presented in Figures 1–8 using 3D surface and contour plots. These visualizations demonstrate the influence of model parameters on key wave characteristics such as amplitude, symmetry, and spatial variation.

As a representative example, the solution v_1 is illustrated in Figure 1. The parameter values used for generating all figures are summarized in Table 1. The plots are generated over the domains $-3 \le x \le 3$ and $-1 \le z \le 1$.

Table 1. Parameter values used for the graphical illustrations in Figures 1–8.

σ	β	k_0	u_0	δ_1	δ_2	r	$p = q$
1.0	0.05	1.0	1.0	0.8	1.0	1	1

The 3D representations show that both the real and imaginary parts exhibit smooth wave-like structures, with periodic variation along the spatial direction x and gradual modulation along z. The real part displays alternating ridges and troughs with relatively symmetric amplitude distribution, while the imaginary part exhibits a similar structure with a noticeable phase shift.

The corresponding contour plots provide additional insight into the spatial structure of the solutions. In particular, the real part exhibits elongated and nearly parallel contour lines, indicating consistent wave propagation. In contrast, the imaginary part shows more curved and interacting contour levels, suggesting a more complex spatial behavior. Together, these plots confirm that the solutions maintain coherent wave structures with both periodic and modulated characteristics.

4.1. Wave structures obtained through the SSM

Across both nonlinear models, the SSM produces three principal classes of traveling-wave solutions:

- **Hyperbolic solutions:** These correspond to localized solitary waves characterized by smooth, non-periodic profiles. They arise when nonlinear and dispersive effects are balanced, allowing coherent propagation.
- **Trigonometric solutions:** These represent spatially periodic wave structures and describe oscillatory dynamics within the medium.
- **Rational solutions:** These solutions exhibit sharp gradients or localized peaks and capture transient or highly nonlinear wave behavior.

The obtained solutions clearly demonstrate the diversity of wave structures supported by the governing equations, reflecting the complex interplay between nonlinearity and dispersion.

4.2. Parameter sensitivity and regime analysis

To further understand the behavior of the obtained solutions, we analyze their sensitivity with respect to key parameters such as b, r, and the wave speed c.

For hyperbolic-type solutions, the parameter b governs the amplitude and steepness of the wave profile. Increasing b results in higher amplitudes and sharper transitions. The parameter r controls the spatial scaling of the traveling coordinate $s = r(x + y - cz)$, and larger values of r lead to narrower and more localized structures.

The wave speed c influences both the propagation direction and the phase structure of the solutions. Variations in c shift the wave profile and modify its spatial evolution.

A critical transition occurs when the parameter b changes sign. For $b > 0$, the solutions are hyperbolic and exhibit localized or kink-type structures. In contrast, for $b < 0$, the solutions become trigonometric, leading to periodic wave behavior. This transition represents a regime shift between localized and oscillatory dynamics.

Furthermore, conditions such as $1 + 4br^2 = 0$ define critical boundaries where the qualitative nature of the solution changes significantly. Near such regimes, the wave profile becomes highly sensitive to parameter variations, leading to noticeable structural deformation.

4.3. Physical interpretation

For the third extended fifth-order nonlinear equation, the hyperbolic solutions correspond to solitary waves commonly observed in dispersive media such as shallow water systems. Their ability to preserve shape during propagation is consistent with classical soliton dynamics. Trigonometric solutions represent periodic wave modes, while rational solutions describe localized transient phenomena.

For the nonlinear electrical transmission line model, the solutions represent voltage propagation along the network. The amplitude corresponds to the voltage magnitude, while the wave speed determines the signal transmission velocity. Localized solutions correspond to stable voltage pulses, whereas periodic solutions describe oscillatory signals observed in resonant circuits.

In this context, the dependent variable $v(x, y, z)$ represents the voltage distribution along the transmission line. The use of complex-valued solutions does not contradict the physical interpretation of the model. In many nonlinear wave systems, complex representations are employed to capture both amplitude and phase information. Observable physical quantities can be obtained from the real part, imaginary part, or magnitude of the solution.

Furthermore, the finite-energy condition

$$Q = \int_{-\infty}^{\infty} |V(s)|^2 \, ds \tag{4.1}$$

represents the total signal power carried by the wave. Finite-energy solutions correspond to stable signal transmission, whereas non-decaying solutions represent background or continuous wave states.

4.4. Quantitative physical measures and stability analysis

To quantitatively characterize the obtained solutions, we introduce two integral measures for the reduced wave profile $V(s)$:

$$M = \int_{-\infty}^{\infty} |V(s)| \, ds, \quad Q = \int_{-\infty}^{\infty} |V(s)|^2 \, ds. \tag{4.2}$$

Finite values of M and Q indicate localization and physical admissibility.

For solutions involving $\operatorname{sech}_{pq}(s)$, the wave profile satisfies

$$\lim_{|s|\to\infty} V(s) = 0, \tag{4.3}$$

and decays exponentially. Therefore, both M and Q are finite, confirming that these solutions correspond to localized finite-energy waves.

In contrast, for solutions of the form

$$V(s) = 3r\sqrt{b}\,\tanh_{pq}(\sqrt{b}s), \tag{4.4}$$

the asymptotic behavior

$$\lim_{|s|\to\infty} V(s) \neq 0 \tag{4.5}$$

implies that

$$M = \infty, \quad Q \to \infty. \tag{4.6}$$

For the first model, this non-decaying behavior is primarily attributed to the presence of linear terms arising from the integration process. These terms grow linearly with the traveling variable s and prevent the solution from satisfying the decay conditions required for localization, resulting in infinite energy.

Accordingly, the obtained solutions can be classified into localized finite-energy waves and non-decaying wave structures.

To examine stability, we consider perturbations of the form

$$v(x, y, z) = V(s) + \epsilon\eta(x, y, z), \tag{4.7}$$

with $\epsilon \ll 1$. Assuming normal-mode perturbations

$$\eta(x, y, z) = e^{\lambda z}\phi(x, y), \tag{4.8}$$

the stability is determined by the sign of $\mathrm{Re}(\lambda)$. If $\mathrm{Re}(\lambda) \leq 0$, the solution is stable; otherwise, it is unstable.

Localized solutions yield bounded coefficients in the linearized problem and thus exhibit stable behavior. In contrast, non-decaying solutions may allow perturbation growth and are therefore more sensitive to disturbances.

Although explicit numerical simulations are not included, the analytical solutions satisfy the governing equations exactly and exhibit behavior consistent with known numerical results. In particular, localized solutions preserve their structure under perturbations and serve as benchmark solutions for validating numerical methods.

All reported solutions have been verified to satisfy the governing equations upon direct substitution.

5. Conclusions

In this study, we applied the SSM to derive analytical solutions for two important nonlinear models: the third extended fifth-order nonlinear equation and the nonlinear electrical transmission line model. These models play a crucial role in describing wave propagation in fluid dynamics and electrical networks, where the interplay between dispersion and nonlinearity produces complex behaviors. Using the SSM, we derived a variety of traveling-wave solutions—including hyperbolic, trigonometric, and rational function forms, which provide deeper insight into the dynamics of the studied models. All obtained solutions were verified through direct substitution into the original governing equations to ensure their correctness and validity. The flexibility of the method in handling complex nonlinear structures underscores its potential as a robust tool for solving higher-order differential equations. Graphical representations of the solutions reveal important features, including wave stability, amplitude variations, and periodic behavior, thereby further validating the method's accuracy. Compared with conventional approaches, the SSM emerges as an efficient and systematic technique for obtaining exact solutions to nonlinear differential equations. Despite these advantages, the method has certain limitations. Its applicability is generally restricted to equations with specific structural forms and depends on the appropriate selection of balance conditions and parameter values. Consequently, while it can generate a wide spectrum of analytical solutions, it may not capture all possible wave structures that can be obtained using alternative approaches, such as transformation or perturbation techniques. In light of these observations, future research may focus on extending and enhancing the SSM to address more complex problems, including coupled systems and higher-dimensional nonlinear models, thereby broadening its applicability in mathematical physics, engineering, and computational sciences. Additionally, integrating analytical results with numerical simulations may provide further validation and improve the practical relevance of the obtained solutions.

Author contributions

Osama Alkhazaleh: Conceptualization, methodology, formal analysis, investigation, writing–original draft, visualization, supervision, project administration; Osama Ala'yed: Methodology, formal analysis, investigation, validation, visualization, writing–review & editing; Abeer M. M. Jaradat: Methodology, formal analysis, investigation, validation, visualization, writing–review & editing. All authors have read and approved the final version of the manuscript for publication.

Use of Generative-AI tools declaration

The authors declare they have not used Artificial Intelligence (AI) tools in the creation of this article.

Conflict of interest

The authors declare no conflict of interest.

References

1. W. Malfliet, Solitary wave solutions of nonlinear wave equations, *Am. J. Phys.*, **60** (1992), 650–654. https://doi.org/10.1119/1.17120

2. O. González-Gaxiola, J. R. de Chávez, Traveling wave solutions of the generalized scale-invariant analog of the KdV equation by tanh–coth method, *Nonlinear Eng.*, **12** (2023), 20220325. https://doi.org/10.1515/nleng-2022-0325

3. O. Ala'yed, New traveling wave solutions of modified Burgers' equations, *Partial Differ. Equ. Appl. Math.*, **13** (2025), 101265. https://doi.org/10.1016/j.padiff.2025.101265

4. M. A. Kayum, M. A. Akbar, M. S. Osman, Stable soliton solutions to the shallow water waves and ion-acoustic waves in a plasma, *Waves Random Complex Media*, **32** (2022), 1672–1693. http://doi.org/10.1080/17455030.2020.1831711

5. M. A. Kayum, S. Ara, M. S. Osman, M. A. Akbar, K. A. Gepreel, Onset of the broad-ranging general stable soliton solutions of nonlinear equations in physics and gas dynamics, *Results Phys.*, **20** (2020), 103762. http://doi.org/10.1016/j.rinp.2020.103762

6. M. E. Islam, H. K. Barman, M. A. Akbar, Search for interactions of phenomena described by the coupled Higgs field equation through analytical solutions, *Opt. Quant. Electron.*, **52** (2020), 468. https://doi.org/10.1007/s11082-020-02583-3

7. R. Roy, M. A. Akbar, A. M. Wazwaz, Exact wave solutions for the time fractional Sharma–Tasso–Olver equation and the fractional Klein–Gordon equation in mathematical physics, *Opt. Quant. Electron.*, **50** (2018), 25. https://doi.org/10.1007/s11082-017-1296-9

8. E. C. Aslan, M. Inc, Optical soliton solutions of the NLSE with quadratic-cubic-Hamiltonian perturbations and modulation instability analysis, *Optik*, **196** (2019), 162661. https://doi.org/10.1016/j.ijleo.2019.04.008

9. R. Roy, M. A. Akbar, A. R. Seadawy, D. Baleanu, Search for adequate closed form wave solutions to space-time fractional nonlinear equations, *Partial Differ. Equ. Appl. Math.*, **3** (2021), 100025. https://doi.org/10.1016/j.padiff.2021.100025

10. W. Y. Guan, B. Q. Li, Mixed structures of optical breather and rogue wave for a variable coefficient inhomogeneous fiber system, *Opt. Quant. Electron.*, **51** (2019), 352. https://doi.org/10.1007/s11082-019-2060-0

11. B. Q. Li, Y. L. Ma, N-order rogue waves and their novel colliding dynamics for a transient stimulated Raman scattering system arising from nonlinear optics, *Nonlinear Dyn.*, **101** (2020), 2449–2461. https://doi.org/10.1007/s11071-020-05906-x

12. Y. L. Ma, Interaction and energy transition between the breather and rogue wave for a generalized nonlinear Schrödinger system with two higher-order dispersion operators in optical fibers, *Nonlinear Dyn.*, **97** (2019), 95–105. https://doi.org/10.1007/s11071-019-04956-0

13. H. M. Baskonus, M. N. Raihen, M. Kayalar, On the extraction of complex behavior of generalized higher-order nonlinear Boussinesq dynamical wave equation and (1+1)-dimensional Van der Waals gas system, *AIMS Mathematics*, **9** (2024), 28379–28399. https://doi.org/10.3934/math.20241377

14. H. U. Rehman, I. Iqbal, S. S. Aiadi, N. Mlaiki, M. S. Saleem, Soliton solutions of the Klein–Fock–Gordon equation using the Sardar subequation method, *Mathematics*, **10** (2022), 3377. https://doi.org/10.3390/math10183377

15. M. Wang, X. Li, J. Zhang, The (G'/G)-expansion method and travelling wave solutions of nonlinear evolution equations in mathematical physics, *Phys. Lett. A*, **372** (2008), 417–423. https://doi.org/10.1016/j.physleta.2007.07.051
16. F. Mahmud, M. Samsuzzoha, M. A. Akbar, The generalized Kudryashov method to obtain exact traveling wave solutions of the PHI-four equation and the Fisher equation, *Results Phys.*, **7** (2017), 4296–4302. https://doi.org/10.1016/j.rinp.2017.10.049
17. H. K. Barman, R. Roy, F. Mahmud, M. A. Akbar, M. S. Osman, Harmonizing wave solutions to the Fokas-Lenells model through the generalized Kudryashov method, *Optik*, **229** (2021), 166294. http://doi.org/10.1016/j.ijleo.2021.166294
18. J. Shen, J. Muhammad, U. Younas, Investigating the wave dynamics and interaction structures: Exploring the Benney–Roskes/Zakharov–Rubenchik model in the oceanic atmosphere, *Ocean Eng.*, **354** (2026), 124969. http://doi.org/10.1016/j.oceaneng.2026.124969
19. I. Siddique, K. B. Mehdi, M. M. M. Jaradat, A. Zafar, M. E. Elbrolosy, A. A. Elmandouh, et al., Bifurcation of some new traveling wave solutions for the time-space M-fractional MEW equation via three altered methods, *Results Phys.*, **41** (2022), 105896. http://dx.doi.org/10.1016/j.rinp.2022.105896
20. K. J. Wang, Exploring exact wave solutions of the Cahn–Allen equation via a novel Bernoulli sub-equation neural networks method, *Modern Phys. Lett. B*, **40** (2026), 2650062. http://doi.org/10.1142/S0217984926500624
21. O. Ozer, H. M. M. Baskonus, H. Bulut, I. Amirali, G. Yel, A new survey to the nonlinear electrical transmission line model, *Int. J. Cogn. Comput. Eng.*, **2** (2021), 208–214. https://doi.org/10.1016/j.ijcce.2021.11.002
22. S. P. Joseph, New traveling wave exact solutions to the coupled Klein–Gordon system of equations, *Partial Differ. Equ. Appl. Math.*, **5** (2022), 100208. https://doi.org/10.1016/j.padiff.2021.100208 .
23. E. Yusufoglu, A. Bekir, Exact solutions of coupled nonlinear Klein–Gordon equations, *Math. Comput. Modellin*, **48** (2008), 1694–1700. https://doi.org/10.1016/j.mcm.2008.02.007
24. S. Akram, M. ur Rahman, L. A. AL-Essa, Bifurcation analysis, chaos, sensitivity, and diverse soliton solutions with propagation insights in a nonlinear spatiotemporal fractional quantum mechanics system, *High Energy Density Phys.*, **57** (2025), 101234. http://doi.org/10.1016/j.hedp.2025.101234
25. P. Guo, X. Wu, L. B. Wang, Multiple soliton solutions for the variant Boussinesq equations, *Adv. Differ. Equ.*, **2015** (2015), 371.
26. A. M. Wazwaz, The extended tanh method for new compact and noncompact solutions for the KP–BBM and the ZK–BBM equations, *Chaos Solitons Fractals*, **38** (2008), 1505–1516. https://doi.org/10.1016/j.chaos.2007.01.135
27. F. B. Pelap, M. M. Faye, Solitonlike excitations in a one-dimensional electrical transmission line, *J. Math. Phys.*, **46** (2005), 033502. https://doi.org/10.1063/1.1843272
28. A. Biswas, C. Zony, E. Zerrad, Soliton perturbation theory for the quadratic nonlinear Klein–Gordon equation, *Appl. Math. Comput.*, **203** (2008), 153–156. http://dx.doi.org/10.1016/j.amc.2008.04.013

29. A. M. Wazwaz, Kink solutions for three new fifth-order nonlinear equations, *Appl. Math. Model.*, **38** (2014), 110–118. http://doi.org/10.1016/j.apm.2013.06.009

30. A. R. Seadawy, D. Yaro, D. Lu, Computational wave solutions of generalized higher-order nonlinear Boussinesq dynamical wave equation, *Modern Phys. Lett. A*, **34** (2019), 1950338. http://doi.org/10.1142/S0217732319503383

31. K. K. Ali, M. S. Mehanna, On some new analytical solutions to the (2+1)-dimensional nonlinear electrical transmission line model, *Eur. Phys. J. Plus*, **137** (2022), 280. http://doi.org/10.1140/epjp/s13360-022-02481-5

32. E. Tala-Tebue, E. M. E. Zayed, New Jacobi elliptic function solutions, solitons and other solutions for the (2+1)-dimensional nonlinear electrical transmission line equation, *Eur. Phys. J. Plus*, **133** (2018), 314. http://doi.org/10.1140/epjp/i2018-12118-7

33. W. M. Taha, M. S. M. Noorani, I. Hashim, New application of the (G′/G)-expansion method for thin film equations, *Abstr. Appl. Anal.*, **2013** (2013), 535138. http://doi.org/10.1155/2013/535138